

Universal modeling of weak antilocalization corrections in quasi-two-dimensional electron systems using predetermined return orbitals

A. Sawada and T. Koga*

Division of Electronics for Informatics, Graduate School of Information Science and Technology, Hokkaido University, Sapporo, Hokkaido 060-0814, Japan

(Received 16 June 2016; revised manuscript received 4 August 2016; published 21 February 2017)

We have developed a method to calculate the weak localization and antilocalization corrections based on the real-space simulation, where we provide 147 885 predetermined return orbitals of quasi-two-dimensional electrons with up to 5000 scattering events that are repeatedly used. Our model subsumes that of Golub [L. E. Golub, *Phys. Rev. B* **71**, 235310 (2005)] when the Rashba spin-orbit interaction (SOI) is assumed. Our computation is very simple, fast, and versatile, where the numerical results, obtained all at once, cover wide ranges of the magnetic field under various one-electron interactions H' exactly. Thus, it has straightforward extensibility to incorporate interactions other than the Rashba SOI, such as the linear and cubic Dresselhaus SOIs, Zeeman effect, and even interactions relevant to the valley and pseudo spin degrees of freedom, which should provide a unique tool to study new classes of materials like emerging 2D materials. Using our computation, we also demonstrate the robustness of a persistent spin helix state against the cubic Dresselhaus SOI.

DOI: [10.1103/PhysRevE.95.023309](https://doi.org/10.1103/PhysRevE.95.023309)

I. INTRODUCTION

It is well-recognized that the weak localization-antilocalization (WL-WAL) effect [1–4] provides a useful tool to study the phase relaxation time and the spin-orbit interaction (SOI) in quasi-two-dimensional electron systems (2DESs) [3,5]. For example, quantitative deductions of the Rashba SOI were performed on 2DESs of III-V compounds [6–8], strained-Ge/SiGe semiconductors [9], and HgTe quantum wells [10] and at the interface or surface of perovskite oxides [11]. The WAL effect, suggesting the existence of the SOI with reasonable strength, has also been observed in graphene [12,13], transition metal dichalcogenides [14], and others [15,16]. Additionally, the SOI provides a key for understanding the novel functionalities in the new class of materials like halide-based perovskite [17] and multiferroics [18,19], where the study of the WL-WAL effect may shed a light on the fundamental understanding of the pertinent materials.

To date, the most “useful” WL-WAL models use the “diffusion approximation” [20,21], which both simplifies the theoretical procedures in k space and provides simple analytical formulas to fit the experimental data. However, these formulas are valid only in small magnetic field ranges for B and B_{SO} , the external magnetic field perpendicular to the 2DES and the magnetic field relevant to the SOI, respectively. In most cases, the criteria is $B, B_{\text{SO}} < B_{\text{tr}}/10$ [22], where B_{tr} is the magnetic field relevant to the transport scattering time τ_{tr} . To describe the magnetoconductivities (MCs) under strong phase relaxation, high magnetic fields and/or high SOI strength, WL-WAL theories beyond the diffusion approximation, based on a ballistic or “Boltzmannian” picture [4] of electrons, are required [23].

In early 1980s, Kawabata implemented the WL model beyond the diffusion approximation for the first time based on the return probability of transport carriers [24,25], which

successfully solved the problem of the experimental deviation from the diffusion model [25]. Some had deemed this discrepancy a result of many-particle interactions, but such contributions are proven to be negligible [26]. Incremental but steady improvements have kept occurring on the WL-WAL models beyond the diffusion approximation in the subsequent 20 yr [6,23,27–32]. In 2005, Golub worked out the WAL model beyond the diffusion approximation analytically taking into account the Rashba-type SOI [33], which provided reliable solutions for the WAL corrections to MCs ($\Delta\sigma$) as a function of the Rashba parameter α . However, it is, in fact, an elaborate task to compute the Golub model numerically for $\Delta\sigma$ as a function of the magnetic field, making this theoretical tool very difficult to use for experimentalists to analyze their experimental data [10].

In this report, we revisit the WAL problem beyond the diffusion approximation from a unique perspective. By looking at the initial development of the theory beyond the diffusion approximation, one can notice that it is the return probability of semiclassical electrons that is directly connected to the WL-WAL effect beyond the diffusion approximation. We will provide a useful set of closed-loop paths generated by a pseudorandom-number generator assuming Boltzmannian electrons that can be used for the calculation of $\Delta\sigma$. We also show a general way to incorporate various one-electron interactions described by Hamiltonian H' happening in each closed-loop path, including the SOI [34,35]. The virtue of our approach is in its straightforward extensibility to incorporate not only the SOI but also the Zeeman effect and other interactions associated with valley degeneracy and/or pseudospin [36], for example, and even multiple of these simultaneously. In the simplest case where only the Rashba SOI is considered, our numerical approach is proven to be equivalent to the Golub model [33]. We have then examined the robustness of the novel spin texture, the so-called “persistent spin helix” (PSH) state [37], when the Rashba and linear- and cubic-Dresselhaus SOIs coexist, as an example of exploring new physics using the framework developed in the present work.

*koga@ist.hokudai.ac.jp

TABLE I. Values associated with the closed loops used for the WL-WAL calculation. The full list is provided in [38]. n_{scat} is the number of scatterings required for the particle to return, where the first “count” is made when it starts the path from the origin. (See Appendix A for the generation of the closed-loop paths using the negative integer values *seed*.)

ν	<i>seed</i>	n_{scat}	S	L	$\cos\varphi'$
1	-12 910	811	125.767	788.021	-0.943 808
2	-16 737	4	0.072 796	1.4435	-0.856 125
\vdots	\vdots	\vdots	\vdots	\vdots	\vdots
147 885	-2 047 996 444	10	0.049 283 3	9.387 79	-0.594 393

II. THEORETICAL DETAILS

The 147 885 closed-loop paths (return orbitals) we will use can be produced using the deterministic feature of a pseudorandom generator, considering the relaxation-time-based (dt/τ_{tr}) Monte Carlo method at constant Fermi velocity v_{F} up to 5000 scattering events with a mean-free-path (MFP) value of dimensionless unity (Table I and Ref. [38]). The length and encircling area of each closed loop can be scaled by the actual MFP value $\ell = v_{\text{F}}\tau_{\text{tr}}$ for obtaining the magnetic field dependence of $\Delta\sigma$. When finding the closed loops, the judgment of “return” was made by watching it pass through a predefined radius Δr around the origin, where $\Delta r = 2.5 \times 10^{-5}$ is used in the present work (Appendix A). The statistics showed that the relative occurrence of a loop with n vertices (scatterings) is proportional to $(n-2)^{-1}$, as predicted theoretically [28].

It is well known that the WL correction to the magnetoconductivity is connected to the areal distribution of the closed loops like those discussed here [2–4]. More specifically, we suggest that F in Eq. (1) of Ref. [28],

$$\Delta\sigma = -\frac{e^2}{2\pi^2\hbar}F, \quad F = 2\pi\ell^2W(0) = \sum_{n=3}^{N_{\text{scat}}} \frac{1}{n-2}, \quad (1)$$

should be read as

$$F = \left(\sum_{n=3}^{N_{\text{scat}}} \frac{1}{n-2} \right) \frac{1}{N_{\text{orbit}}} \sum_{j=1}^{N_{\text{orbit}}} \cos\left(2\pi \frac{BS_j\ell^2}{h/2e}\right), \quad (2)$$

considering the loops up to N_{scat} ($=5000$) vertices (scatterings), where N_{orbit} is the number of orbitals we pick randomly from the predefined 147 885 orbitals ($N_{\text{orbit}} \leq 147\,885$) and S_j (dimensionless quantity) is the encircling area of the j th orbital (Fig. 1). We note $\frac{1}{N_{\text{orbit}}} \sum_{j=1}^{N_{\text{orbit}}} \cos\left(2\pi \frac{BS_j\ell^2}{h/2e}\right) = 1$ for $B = 0$. All

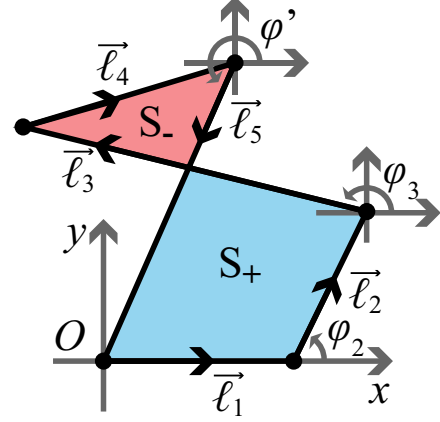


FIG. 1. Closed-loop path with $n_{\text{scatt}} = 5$. This consists of line segments \vec{l}_1 , \vec{l}_2 , \vec{l}_3 , \vec{l}_4 , and \vec{l}_5 . Note that the total ballistic length L and the encircling area S of this loop are given as $L = \sum_{i=1}^{n_{\text{scat}}} |\vec{l}_i|$ and $S = |S_+ - S_-|$, respectively, where both S_+ and S_- are defined to be positive (see Ref. [35]).

the corrections required to make Eq. (1) fully equivalent to the most updated Cooperon-based WL-WAL theories beyond the diffusion approximation are (1) the incorporation of the phenomenological phase relaxation, (2) the nonbackscattering correction [31,32], and (3) the incorporation of various one-electron interactions, whose Hamiltonian is H'_k , including the SOI and Zeeman effect. For doing this, we put the factor x_j below in front of $\cos\left(2\pi \frac{BS_j\ell^2}{h/2e}\right)$ in Eq. (2), i.e.,

$$\sum_{j=1}^{N_{\text{orbit}}} x_j \cos\left(2\pi \frac{BS_j\ell^2}{h/2e}\right),$$

$$x_j = \exp\left(-\frac{L_j}{L_\phi}\right) \times \frac{1}{2} \text{Re}[\text{Tr}\{\mathbf{U}_{\text{CCW},j}^\dagger \mathbf{U}_{\text{CW},j}\}] \times (1 + \cos\varphi'_j), \quad (3)$$

where L_j , L_ϕ , and φ'_j are the total ballistic length (sum of the line segments) for the j th loop (L in Table I), the ballistic phase relaxation length defined by $v_{\text{F}}\tau_\phi$ (τ_ϕ being the phase relaxation time) [39], and the azimuthal angle for the returning electron, respectively (see Fig. 1). We follow Ref. [32] for the incorporation of the nonbackscattering correction $(1 + \cos\varphi'_j)$ [40]. The vector representations of the first and last segments of the closed loop are $\vec{l}_1 = (l_1 \cos\varphi_1, l_1 \sin\varphi_1)$ and $\vec{l}_{n_{\text{scat}}} = (l_{n_{\text{scat}}} \cos\varphi', l_{n_{\text{scat}}} \sin\varphi')$, respectively, where φ_1 is set to zero making use of the circular symmetry in the present work (see Fig. 1).

The propagators \mathbf{U}_{CW} and \mathbf{U}_{CCW} are most generally written as

$$\mathbf{U}_{\text{CW}} = \mathbf{S}_{\mathbf{k}_1, \mathbf{k}_{j_{\text{scat}}}}^{\text{imp}} \exp\left(-i \frac{H'_{\mathbf{k}_{j_{\text{scat}}}}}{\hbar} t_{n_{\text{scat}}}\right) \cdots \mathbf{S}_{\mathbf{k}_3, \mathbf{k}_2}^{\text{imp}} \exp\left(-i \frac{H'_{\mathbf{k}_2}}{\hbar} t_2\right) \mathbf{S}_{\mathbf{k}_2, \mathbf{k}_1}^{\text{imp}} \exp\left(-i \frac{H'_{\mathbf{k}_1}}{\hbar} t_1\right),$$

$$\mathbf{U}_{\text{CCW}} = \mathbf{S}_{-\mathbf{k}_{j_{\text{scat}}}, -\mathbf{k}_1}^{\text{imp}} \exp\left(-i \frac{H'_{-\mathbf{k}_1}}{\hbar} t_1\right) \mathbf{S}_{-\mathbf{k}_1, -\mathbf{k}_2}^{\text{imp}} \exp\left(-i \frac{H'_{-\mathbf{k}_2}}{\hbar} t_2\right) \cdots \mathbf{S}_{-\mathbf{k}_{j_{\text{scat}}-1}, -\mathbf{k}_{j_{\text{scat}}}}^{\text{imp}} \exp\left(-i \frac{H'_{-\mathbf{k}_{j_{\text{scat}}}}}{\hbar} t_{n_{\text{scat}}}\right),$$

where $\mathbf{S}_{\mathbf{k},\mathbf{k}'}^{\text{imp}}$ is the quantum mechanical operation associated with the scattering of electrons from state \mathbf{k} to state \mathbf{k}' and t_i is the time required for the electron to move in the i th segment ($t_i = l_i/v_F$ in the simplest case). We note that the successive accumulation of the quantum mechanical phase, $\exp[2i\varphi(r,r') - 2i\tau\mathbf{S} \cdot \boldsymbol{\omega}(\mathbf{R})]$ in Eq. (8) of Ref. [33], leads to both the cos term and $\frac{1}{2}\text{Re}[\text{Tr}\{\mathbf{U}_{\text{CCW},j}^\dagger \mathbf{U}_{\text{CW},j}\}]$, in Eqs. (2) and (3), respectively, where $\mathbf{S}_{\mathbf{k},\mathbf{k}'}^{\text{imp}}$ is set to be a unit matrix. We further note that the effect of spin precession is incorporated as a constant precession angle ($\propto \tau$) for all segments of the electron passage in Ref. [33], whereas the spin precession angles in the present work are proportional to the length of each segment ($\propto t_n, n = 1, 2, 3, \dots$), a clear improvement from Ref. [33]. We also reiterate that various interactions, not only the Rashba-Dresselhaus SOIs and the Zeeman effect, but also anisotropic scattering, intervalley scattering, and/or interactions associated with the pseudospin degree of freedom (as in 2D materials including graphene) can be incorporated straightforwardly in our scheme through $\frac{1}{2}\text{Re}[\text{Tr}\{\mathbf{U}_{\text{CCW},j}^\dagger \mathbf{U}_{\text{CW},j}\}]$ (see Appendix B for the derivation), which has never been possible in the currently available Cooperon-base formalisms [33,36]. Our approach is similar in taste to Ref. [32], where randomly distributed hard-core scatterers were used to generate closed-loop paths for the calculation of WL without being able to incorporate one electron interaction $H_{\mathbf{k}}'$. The distribution of the closed-loop paths in our approach reflects exactly that of the analytical formalism found in Refs. [24,25,28]. The computation in our approach is also much simpler than that in Ref. [32].

To evaluate Eq. (1) as a function of B most efficiently, we make a histogram of counts out of the N_{orbit} loops according to the encircling area S (dimensionless quantity) with the areal interval ΔS ($\Delta S = 0.1$ in the present work). We assume S values to be positive numbers here because only their absolute values are important in the subsequent calculations. The i th bin in the histogram thus created, denoted as $w_0[i]$, contain the number of loops whose S falls in the range $(i - 0.5) < S/\Delta S < (i + 0.5)$. To obtain $\Delta\sigma$ as a function of B perpendicular to the 2DES plane, we use the standard FFT algorithm to convert $w_0[i]$ to $w_0[i]_{\text{FFTed}}$ [41]. We set the array size of $w_0[i]$ to be $2^N + 1$ (typically $N = 17$) for this purpose [42]. We also note that the correct FFT conversion here should produce $w_0[0]_{\text{FFTed}} = 147\,885$ or N_{orbit} , which should be used as a check of the FFT procedure.

We now have

$$\Delta\sigma[i] = -\frac{e^2}{2\pi^2\hbar} \times F_0 \times \frac{w_0[i]_{\text{FFTed}}}{N_{\text{orbit}}}, \quad (4)$$

$$B[i] = \frac{i}{2^N} \times \frac{\pi}{\Delta S} B_{\text{tr}}, \quad (5)$$

where $B_{\text{tr}} = \hbar/2e\ell^2$, $F_0 = \{\sum_{n=3}^{N_{\text{scat}}} (n-2)^{-1}\}$ is the theoretical return probability considering up to N_{scat} scatterings [28] and N_{orbit} is the number of orbits used to make the histogram $w_0[i]$. In the present work, $N_{\text{scat}} = 5000$ ($F_0 = 9.0941$) and $N_{\text{orbit}} = 147\,885$. However, one can use any smaller numbers of N_{orbit} to reduce the computation time, though the statistical reliabilities of the final results decrease (see Sec. IV) [43]. We also note that the integer i ($0 \leq i \leq 2^N$) connects $\Delta\sigma$ and

B . Equations (4) and (5) provide reliable numerical values for the WL correction in a quasi-2DES for an abrupt phase relaxation at 5000 scatterings. In order to include the correction by Eq. (3), the i th bin of the histogram $w_0[i]$ should be replaced with $\sum_{j=1}^{N_i} x_j$, where j is now an index attached to a loop that belongs to the i th histogram bin and N_i is the total number of the closed loops in this bin. Once we set the histogram $w[0, \dots, 2^N]$, we can obtain $\Delta\sigma[0, \dots, 2^N]$ just in the same way as above, where $w_0[i]_{\text{FFTed}}$ is now replaced with $w[i]_{\text{FFTed}}$, which is the FFT of $w[i]$ [41].

Let us now elaborate the relatively simple case where the interaction is only spin rotation by the SOI. Any of the SOI or Zeeman-type Hamiltonians or even arbitrary combinations of these have the following general form.

$$H_{\text{SOI,B}} = \tilde{\mathbf{B}}(\mathbf{k}, \mathbf{B}) \cdot \boldsymbol{\sigma}. \quad (6)$$

For example, $\tilde{\mathbf{B}}(\mathbf{k}, \mathbf{B}) = (\alpha k_y, -\alpha k_x)$ for the Rashba Hamiltonian [$H_{\text{R}} = \alpha(k_y\sigma_x - k_x\sigma_y)$], where α is the Rashba SOI coefficient, and $\tilde{\mathbf{B}} = (-\frac{1}{2}g\mu_{\text{B}}B_x, -\frac{1}{2}g\mu_{\text{B}}B_y)$ for the Zeeman Hamiltonian [$H_{\text{Z}} = -\frac{1}{2}g\mu_{\text{B}}\mathbf{B} \cdot \boldsymbol{\sigma}$], where g and μ_{B} are the effective g value and Bohr magneton, respectively ($\mathbf{B} \perp \hat{z}$ is assumed for simplicity). The spin rotation axis $\hat{\xi}(\mathbf{k}, \mathbf{B})$ and angle $\theta(\mathbf{k}, \mathbf{B})$ under the Hamiltonian in Eq. (6) for an electron traveling a distance l are given as $\tilde{\mathbf{B}}(\mathbf{k}, \mathbf{B})/|\tilde{\mathbf{B}}(\mathbf{k}, \mathbf{B})|$ and $2|\tilde{\mathbf{B}}(\mathbf{k}, \mathbf{B})|l/\hbar v_F$, respectively. Thus, the spin rotation operator

$$\begin{aligned} \mathbf{R}_{\hat{\xi}}(\theta) &= \mathbf{I} \cos \frac{\theta}{2} - i \hat{\xi}(\mathbf{k}, \mathbf{B}) \cdot \boldsymbol{\sigma} \sin \frac{\theta}{2} \\ &= \begin{pmatrix} \cos(\theta/2) & -i\xi_- \sin(\theta/2) \\ -i\xi_+ \sin(\theta/2) & \cos(\theta/2) \end{pmatrix}, \end{aligned} \quad (7)$$

where $\xi_{\pm} = \xi_x \pm i\xi_y$ [34], in the present case reads

$$\mathbf{R}_{\hat{\xi}}(\theta) = \begin{pmatrix} \cos(k_{\alpha}l) & (k_-/k) \sin(k_{\alpha}l) \\ (k_+/k) \sin(k_{\alpha}l) & \cos(k_{\alpha}l) \end{pmatrix}. \quad (8)$$

The expression of $\mathbf{R}_{\hat{\xi}}(\theta)$ for the case of the cubic Dresselhaus Hamiltonian is given in Appendix C. In Eq. (8), $k_{\pm} = k_x \pm ik_y$ and $k_{\alpha} = \frac{\alpha m^*}{\hbar^2}$ (m^* being the effective mass). The total spin rotation operator \mathbf{R}_{tot} for a closed-loop path is then given as

$$\mathbf{R}_{\text{tot}} = \mathbf{R}_{\hat{\xi}_{n_{\text{scat}}}}(\theta_{n_{\text{scat}}}) \cdots \mathbf{R}_{\hat{\xi}_2}(\theta_2) \mathbf{R}_{\hat{\xi}_1}(\theta_1). \quad (9)$$

$\frac{1}{2}\text{Re}[\text{Tr}\{\mathbf{U}_{\text{CCW},j}^\dagger \mathbf{U}_{\text{CW},j}\}]$ in Eq. (3) now reduces to $\frac{1}{2}\text{Tr}\{\mathbf{R}_{\text{tot}}^2\}$ [35], where $\text{Tr}\{\mathbf{A}\}$ is the trace of matrix \mathbf{A} , if \mathbf{R}_{tot} has the time-reversal symmetry as in the case of the spin rotation by the SOI Hamiltonians only (see Appendix B).

III. RESULTS

Shown in Fig. 2(a) are the image plot of the calculated $\Delta\sigma$ assuming the Rashba SOI and $L_{\phi} = 10$ (dimensionless length used in this simulation) [44] as a function of $\theta_{\text{R}} = 2k_{\alpha}\ell$ and the normalized magnetic field B/B_{tr} , where θ_{R} is the spin rotation angle per the MFP length and $B_{\text{tr}} = \frac{\hbar}{2e\ell^2}$ (see Appendix D for the results with other L_{ϕ} values). It is noted that computation time required to generate the whole data in Fig. 2(a) is on the order of minutes using an inexpensive modern desktop computer.

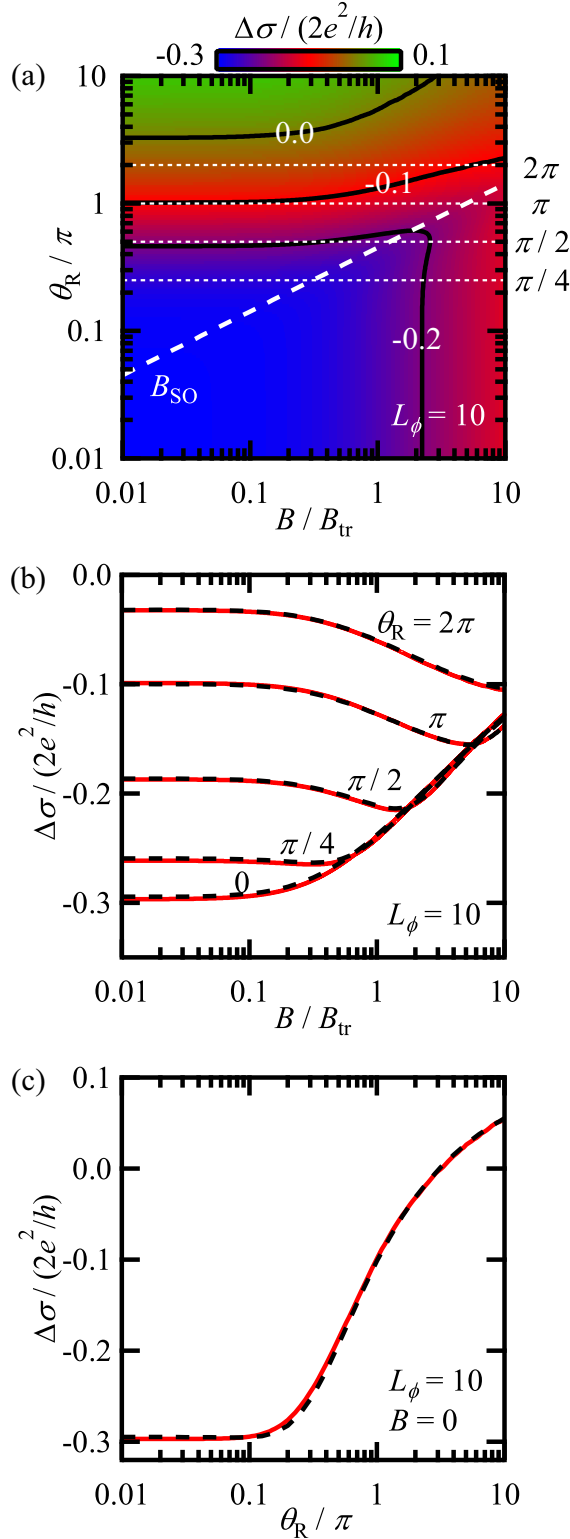


FIG. 2. (a) Image plot of the calculated $\Delta\sigma$ as a function of the magnetic field B and spin rotation angle per the MFP value θ_R . The position of $B_{SO} \equiv \theta_R^2 B_{tr}/2$ is indicated by the white dashed line. (b) Cuts (cross sections) of the image plot at $\theta_R = 0, \pi/4, \pi/2, \pi$, and 2π (red solid curves) together with the corresponding results by the Golub model (black dashed curves) [45]. (c) θ_R dependence of $\Delta\sigma$ calculated by our model (red solid curve) and the Golub model (black dashed curve) at $B = 0$. All the results here [(a)–(c)] were obtained using $L_\phi = 10$ for the phase relaxation.

To have a closer look at Fig. 2(a), cuts (cross sections) of the image plot at $\theta_R = 0, \pi/4, \pi/2, \pi$, and 2π are shown in Fig. 2(b) together with the results of the Golub model using the same parameter values for θ_R and L_ϕ , where we see exact agreement between the results in the present work and those of the Golub model [45]. The result for $\theta_R = 0$ denotes the WL curve (without SOI). It is noted that the computation time we needed to generate the five curves for the Golub model in Fig. 2(b) was on the order of hours using the same desktop computer as above, because the implementation of the Golub model is so cumbersome [10]. It is also noted that approximated formulas exist based on the Golub model for the values of $\Delta\sigma$ at $B = 0$ as a function of B_{SO} , where $B_{SO} = \theta_R^2 B_{tr}/2$ [see Fig. 2(c)] [33]. A very small discrepancy seen in Fig. 2(c) around $\theta_R = 0.3\pi$ between the results of the approximated formulas and the present results turned out to be due to the errors in the approximated formulas, not in the present results [46].

We now explore new physics using the method developed in this work, which had never been possible in other frameworks of the WL-WAL theory beyond the diffusion approximation. The coexistence of the Rashba and linear- and cubic-Dresselhaus SOIs provides intriguing problems in semiconductor spintronics. For example, in top-gated (001)InP lattice-matched InGaAs quantum wells, Faniel *et al.* [7] found that the Dresselhaus SOIs are essentially negligible unless α is vanishingly small, while Yoshizumi *et al.* [47] recently observed a clear separation in the WL-WAL measurements between the two distinct PSH states [37] corresponding to $\alpha = \pm\beta_1$ (see below for the meaning of β_1), despite the existence of a finite cubic Dresselhaus SOI. In the following investigation, we define the linear Dresselhaus Hamiltonian as $H_D^{(1)} = \beta_1(k_x\sigma_x - k_y\sigma_y)$ so that the corresponding spin rotation angle per the MFP length is $\theta_{D1} = 2\beta_1 m^* \ell / \hbar^2$. The cubic Dresselhaus SOI is discussed in Appendix C, and the corresponding spin rotation angle per the MFP length is denoted as θ_{D3} . Now, our Hamiltonian $H' = H_R + H_D^{(1)} + H_D^{(3)}$ does not retain the circular symmetry anymore. On the other hand, it was based on the circular symmetry that we set $\varphi_1 = 0$ in our computation. To resolve this problem, the k_x - k_y coordinate in Hamiltonian should be rotated by an arbitrary (random) angle in each closed loop in calculating Eq. (3). We also fix the value of L_ϕ at 100 here.

Shown in Fig. 3(a) is the image plot of the WL curves for the PSH states ($\theta_R = \theta_{D1}, \theta_{D3} = 0$), where the ordinate is θ_R (or θ_{D1}) and the abscissa is B/B_{tr} . All MC curves with different θ_R values are identical to one another, as expected. An intriguing question is how these PSH states would be broken by the introduction of finite cubic Dresselhaus SOI. Shown in Figs. 3(b) and 3(c) are the image plots of WL-WAL curves with $\theta_R = \theta_{D1}$, but $\theta_{D3} = \pi/64$ and $\theta_{D3} = \pi/16$, respectively. A surprising fact is that the larger the value of θ_R (or θ_{D1}), the more robust the PSH state is against the incorporation of the cubic Dresselhaus SOI. For example, as in Fig. 3(b), if θ_{D3} is as small as $\pi/64$, all MC curves remain WL-like, but the WL curves are increasingly affected by θ_{D3} as the value of θ_R is reduced. If the value of θ_{D3} is increased to $\pi/16$ [Fig. 3(c)], we observe the transition from WL-like MC curves to WAL-like MC curves as we decrease the value of θ_R from 10π to 0.01π , where its boundary is around $\theta_R = 5\pi$.

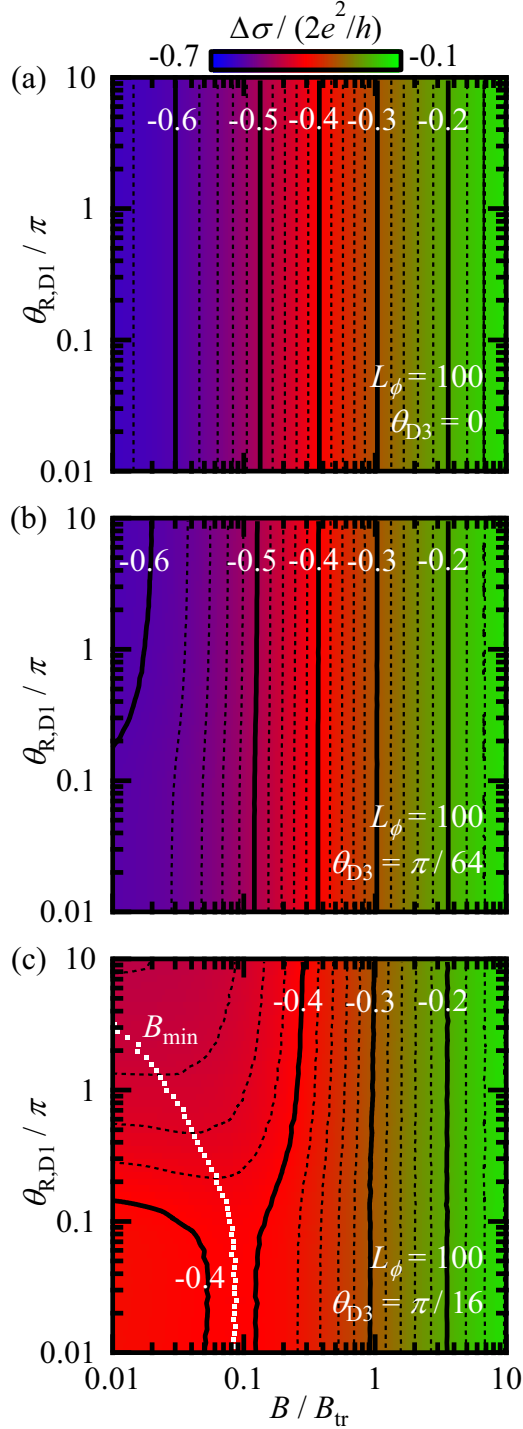


FIG. 3. Image plots of the calculated $\Delta\sigma$ as a function of the magnetic field B (abscissa) and spin rotation angle per the MFP value θ_R (ordinate) assuming $\theta_R = \theta_{D1}$, with $L_\phi = 100$. Panel (a) denotes the result of the persistent spin helix states ($\theta_{D3} = 0$). Panels (b) and (c) denote the results for $\theta_{D3} = \pi/64$ and $\pi/16$, respectively. In (c), B_{\min} (white dots) denotes the magnetic fields at which $\Delta\sigma(B)$ becomes locally minimum.

IV. DISCUSSIONS

Let us now consider the statistical reliability of $\Delta\sigma$ in the presence of an external magnetic field B in the present work.

The contribution to $\Delta\sigma$ from a randomly picked closed loop, indexed by j , is given as

$$-\frac{e^2 F_0}{2\pi^2 \hbar N_{\text{orbit}}} \times x_j \times \cos\left(2\pi \frac{BS_j \ell^2}{h/2e}\right), \quad (10)$$

where the front prefactor ($-\frac{e^2 F_0}{2\pi^2 \hbar N_{\text{orbit}}}$) is found in Eq. (4), x_j is given in Eq. (3), and the last part is from the wave function interference due to the vector potential responsible for B . It is noted that BS_j is the magnetic flux piercing the loop, S_j is the encircling area of the loop j , and $h/2e$ is a half of the magnetic flux quantum. Calling the quantity of Eq. (10), with removing N_{orbit} in the denominator, as $X_j(B)$ and changing the index j to ν to refer to all closed loops, i.e., $1 \leq \nu \leq N_{\text{orbit}}$ (as in Table I or [38]), we can now write

$$\Delta\sigma(B) = \frac{1}{N_{\text{orbit}}} \sum_{\nu=1}^{N_{\text{orbit}}} X_\nu(B) \equiv \langle X_\nu(B) \rangle_{N_{\text{orbit}}}. \quad (11)$$

The statistical deviation of $\Delta\sigma(B)$ from the true value is assessed as

$$\delta\Delta\sigma(B) = \sqrt{\frac{\langle X_\nu(B)^2 \rangle_{N_{\text{orbit}}} - \langle X_\nu(B) \rangle_{N_{\text{orbit}}}^2}{N_{\text{orbit}}}}. \quad (12)$$

Appendix E shows that $\delta\Delta\sigma(B)$ (we write this simply $\delta\Delta\sigma$ hereafter) can be evaluated using a histogram $w_2[i]$, defined as $w_2[i] = \sum_{j=1}^{N_i} x_j^2$, where the same histogram interval as in $w[i]$ and x_j found in Eq. (3) were used. The final result is

$$\delta\Delta\sigma[i] = \frac{e^2 F_0}{2\pi^2 \hbar \sqrt{N_{\text{orbit}}}} \sqrt{\frac{w_2[0]_{\text{FFTed}} + w_2[i]_{\text{FFTed}}}{2N_{\text{orbit}}}}, \quad (13)$$

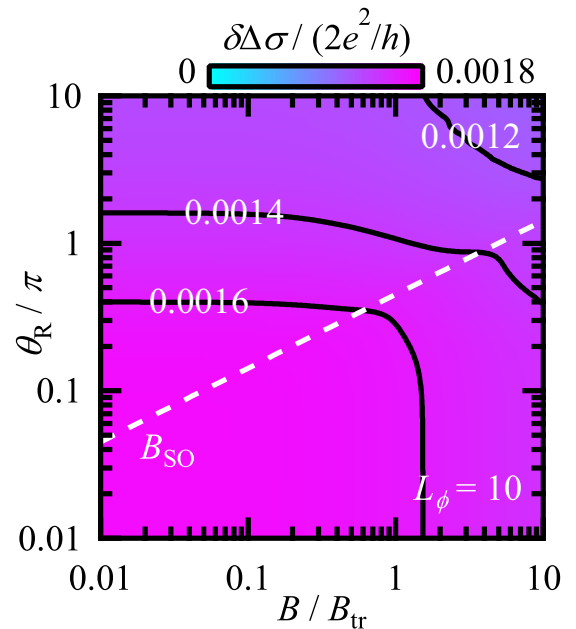


FIG. 4. Image plot of the estimated statistical errors for the values of $\Delta\sigma$ in Fig. 2(a), denoted as $\delta\Delta\sigma$, as a function of θ_R and B . We used $N_{\text{orbit}} = 147885$ and $L_\phi = 10$. The position of $B_{\text{SO}} \equiv \theta_R^2 B_{\text{tr}}/2$ is indicated by the white dashed line.

with $B[i] = \frac{i}{2^N} \times \frac{\pi B_{\text{fit}}}{2\Delta S}$, where $w_2[0, \dots, 2^N]_{\text{FFTed}}$ is the FFT of $w_2[0, \dots, 2^N]$ [41]. We note that $B[i]$ here is different from Eq. (5) by a factor of a half.

We show the calculated image plot of $\delta\Delta\sigma$ in Fig. 4 using $N_{\text{orbit}} = 147885$ and $L_\phi = 10$. Comparing this with Fig. 2(a), we find that $\delta\Delta\sigma$ is typically 1% or smaller of $\Delta\sigma$ for all parameter values of θ_R and B . We also note that $\delta\Delta\sigma \propto 1/\sqrt{N_{\text{orbit}}}$. Therefore, reducing the number of loops to be used in the calculation from 147 885 to $N_{\text{orbit}} = 10000$ will increase the computation speed by a factor of 15, whereas the increase in $\delta\Delta\sigma$ is only by a factor of 4 or less. Thus, good numerical reliability is kept even with $N_{\text{orbit}} = 10000$ for the purpose of fitting the experimental data.

V. CONCLUSIONS

We have developed a unique numerical method to calculate the WAL corrections to the magnetoconductivity of 2DES beyond the diffusion approximation. This approach uses a single collection of closed-loop paths, generated by a pseudorandom-number generator. Because of the scalable nature of 2DES, the WAL corrections of any 2DESs can be described by this single collection of the loops provided the Boltzmannian picture is valid to describe the given electrons. Our approach subsumes that of Golub [33], if we consider only the Rashba spin-orbit interaction as possible one-electron interactions in the system. We then numerically examined the robustness of the persistent spin helix states in degenerate semiconductor quantum wells against the incorporation of the cubic Dresselhaus Hamiltonian as an example of exploring new physics using the newly developed theoretical framework in the present work. Our approach can be extended to incorporate interactions other than the spin-orbit interaction in a straightforward way, such as the Zeeman effect and those associated with the valley and pseudospin degrees of freedom. Thus, our approach should be also useful in the research of class of emerging 2D materials.

ACKNOWLEDGMENTS

The authors are indebted to Professors K. Yakubo, H. Suzuura, A. Sakai, J. C. Egues, J. J. Heremans, M. Kohda, and T. Asai for fruitful discussions. This work was supported by JSPS KAKENHI Grant No. 16H01045.

APPENDIX A: GENERATION OF CLOSED-LOOP PATHS

The 147 885 closed-loop paths used in the present work can be generated using the pseudorandom-number generator “double ran1(int &)” defined in Ref. [48]. The source code of “double ran1(int &)” is reproduced below for the convenience of the readers.

```
double ran1(int &idum){//numerical recipe in C++
  const int IA=16807, IM=2147483647, IQ=127773,
          IR=2836, NTAB=32;
  const int NDIV=(1+(IM-1)/NTAB);
  const double EPS=3.0e-16, AM=(1.0/IM),
          RNMX=(1.0-EPS);
  static int iy = 0;
  static int iv[NTAB];
  int j, k;
  double temp;
  if (idum <= 0 || !iy){
    if (-idum < 1) idum = 1;
    else idum = -idum;
    for(j=NTAB+7;j>=0;j--){
      k=idum/IQ;
      idum=IA*(idum-k*IQ)-IR*k;
      if (idum<0) idum += IM;
      if (j<NTAB) iv[j] = idum;
    }
    iy = iv[0];
  }
  k=idum/IQ;
  idum=IA*(idum-k*IQ)-IR*k;
  if (idum<0) idum += IM;
  j = iy / NDIV;
  iy = iv[j];
  iv[j] = idum;
  if ((temp = AM*iy) > RNMX) return (float)RNMX;
  else return temp;
}
```

For readers to check whether this code is working exactly in the same way as in our work, we provide the output of the following main program. The output values are 0.464 514, 0.928 778, and 0.502 077.

```
#include <iostream>
using namespace std;

main(){
  int i, seed=-1000;
  ran1(seed); // initialization of ran1()
  for(i=0;i<3;i++) cout << ran1(seed) << endl;
}
```

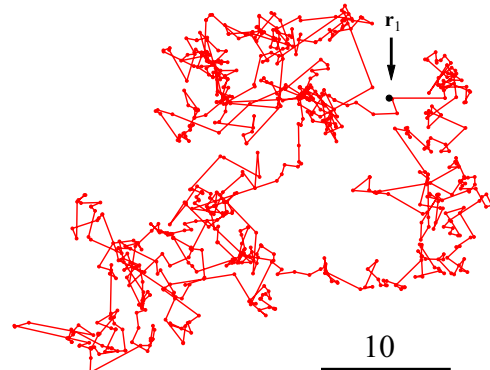


FIG. 5. A plot of an actual orbital (closed-loop path) for $seed = -12910$.

Then, the closed loop for $\nu = 1$ in Table I, for example, can be generated by the following code (based on the Monte Carlo type 2D random walk of Boltzmannian electron).

```
#include <iostream>
using namespace std;

main(){
    int seed = -12910, n_scatter = 811, i_scatter;
    double x, y, length, theta ;
    ran1(seed) ; //initialize ran1()

    // i_scatter = 1
    x = 0 ; y = 0 ;
    cout << x << "\t" << y << endl ;

    // i_scatter = 2
    x = -log(ran1(seed)) ; y = 0 ;
    cout << x << "\t" << y << endl ;

    //i_scatter >=3
    for( i_scatter=3 ; i_scatter<=n_scatter+1 ; i_scatter++)
    {
        length = -log( ran1(seed)) ;
        theta = 2.0*M_PI*ran1(seed) ;
        x += length*cos(theta) ;
        y += length*sin(theta) ;
        cout << x << "\t" << y << endl ;
    }
}
```

The plot of the coordinate data generated from the above code is shown in Fig. 5, where the last point was replaced with $\mathbf{r}_1 = (0,0)$.

Some of the numerical data generated from the code above are given in Table II. We note that the definition of our *return* is “the electron passes by the origin with a closest distance between them that is smaller than some predefined Δr ”. We chose $\Delta r = 2.5 \times 10^{-5}$ in the present work. While the value of Δr can be chosen rather arbitrarily if it is sufficiently small, the finiteness in Δr surely serves as the

TABLE II. Positions of scatterings for seed = -12910.

i_{scatter}	x	y
1	0	0
2	4.437 93	0
3	4.348 36	0.643 426
4	4.343 45	0.620 36
5	5.139 98	1.152 97
6	4.182	0.830 371
7	3.874 29	1.041 73
⋮	⋮	⋮
807	-3.319 09	-0.579 836
808	-2.622 21	-0.350 079
809	-1.265 27	-1.284 92
810	0.632 24	-1.218 75
811(n_{scatter})	0.238 902	-0.083 656 5
812($n_{\text{scatter}} + 1$)	-0.4707	0.164 902

source of errors to the final results. These errors are almost exclusively caused by (1) the multiple returns of the particle from the same initial condition within 5000 scatterings (or N_{scatter}) and (2) the nonrigorous definition of the “return” condition. The quantitative corrections to these errors were considered elsewhere [49]. With such error corrections, we can obtain almost error-free final results with Δr values even as large as 5×10^{-2} .

APPENDIX B: DERIVATION OF THE ONE-ELECTRON INTERACTION CORRECTION WITHOUT TIME-REVERSAL SYMMETRY

Let us write the scattering sequence of a closed-loop path in the clockwise (CW) and counterclockwise (CCW) directions as

$$\begin{aligned} \text{CW} : \mathbf{r}_1 \xrightarrow{\mathbf{k}_1} \mathbf{r}_2 \xrightarrow{\mathbf{k}_2} \dots \xrightarrow{\mathbf{k}_{n-1}} \mathbf{r}_n \xrightarrow{\mathbf{k}_n} \mathbf{r}_1, \\ \text{CCW} : \mathbf{r}_1 \xrightarrow{-\mathbf{k}_n} \mathbf{r}_n \xrightarrow{-\mathbf{k}_{n-1}} \dots \xrightarrow{-\mathbf{k}_2} \mathbf{r}_2 \xrightarrow{-\mathbf{k}_1} \mathbf{r}_1. \end{aligned}$$

Let \mathbf{U}_{CW} and \mathbf{U}_{CCW} be the one-electron interaction propagator associated with the closed loops of the Boltzmannian electron in the CW and CCW directions, respectively. Here, we do not assume $\mathbf{U}_{\text{CW}} = \mathbf{U}_{\text{CCW}}^{-1} = \mathbf{U}_{\text{CW}}^\dagger$ because the time-reversal symmetry is not taken for granted.

We consider the amplitude of the wave function interference (for example, spin interference) using the wave functions $\psi_{\text{CW}} = \exp(2i\pi \frac{BS}{h/e})\mathbf{U}_{\text{CW}}|i\rangle$ and $\psi_{\text{CCW}} = \exp(-2i\pi \frac{BS}{h/e})\mathbf{U}_{\text{CCW}}|i\rangle$, where $|i\rangle$ is the initial electronic state at \mathbf{r}_1 including multiple degrees of freedom reflecting various one-electron interactions including spin,

$$\begin{aligned} & \left| \frac{1}{\sqrt{2}}(\psi_{\text{CW}} + \psi_{\text{CCW}}) \right|^2 \\ &= \frac{1}{2} \{ |\psi_{\text{CW}}|^2 + |\psi_{\text{CCW}}|^2 + \psi_{\text{CCW}}^\dagger \psi_{\text{CW}} + \psi_{\text{CW}}^\dagger \psi_{\text{CCW}} \} \\ &= 1 + \frac{1}{2} \{ (e^{-2\pi i \frac{BS}{h/e}} \mathbf{U}_{\text{CCW}}|i\rangle)^\dagger (e^{2\pi i \frac{BS}{h/e}} \mathbf{U}_{\text{CW}}|i\rangle) \\ & \quad + (e^{2\pi i \frac{BS}{h/e}} \mathbf{U}_{\text{CW}}|i\rangle)^\dagger (e^{-2\pi i \frac{BS}{h/e}} \mathbf{U}_{\text{CCW}}|i\rangle) \} \\ &= 1 + \frac{1}{2} \{ e^{2\pi i \frac{BS}{h/2e}} \langle i | \mathbf{U}_{\text{CCW}}^\dagger \mathbf{U}_{\text{CW}} | i \rangle \\ & \quad + e^{-2\pi i \frac{BS}{h/2e}} \langle i | \mathbf{U}_{\text{CW}}^\dagger \mathbf{U}_{\text{CCW}} | i \rangle \} \\ &= 1 + \text{Re} \{ e^{2\pi i \frac{BS}{h/2e}} \langle i | \mathbf{U}_{\text{CCW}}^\dagger \mathbf{U}_{\text{CW}} | i \rangle \} \\ &= 1 + \cos \left(2\pi \frac{BS}{h/2e} \right) \text{Re} \{ \langle i | \mathbf{U}_{\text{CCW}}^\dagger \mathbf{U}_{\text{CW}} | i \rangle \} \\ & \quad - \sin \left(2\pi \frac{BS}{h/2e} \right) \text{Im} \{ \langle i | \mathbf{U}_{\text{CCW}}^\dagger \mathbf{U}_{\text{CW}} | i \rangle \}, \end{aligned}$$

where we neglect the last term since it will be averaged out by taking into account contributions from all closed loops and letting the encircling area S now have a sign (not always positive). We also let $|i\rangle = \begin{pmatrix} e^{-i\phi/2} \cos \frac{\theta}{2} \\ e^{i\phi/2} \sin \frac{\theta}{2} \end{pmatrix}$, $\mathbf{U}_{\text{CW}} = \begin{pmatrix} U_{\text{CW},00} & U_{\text{CW},01} \\ U_{\text{CW},10} & U_{\text{CW},11} \end{pmatrix}$, and $\mathbf{U}_{\text{CCW}} = \begin{pmatrix} U_{\text{CCW},00} & U_{\text{CCW},01} \\ U_{\text{CCW},10} & U_{\text{CCW},11} \end{pmatrix}$ considering only the spin degree of freedom.

Then,

$$\begin{aligned} \langle i | \mathbf{U}_{\text{CCW}}^\dagger \mathbf{U}_{\text{CW}} | i \rangle &= \cos^2 \frac{\theta}{2} (U_{\text{CCW},00}^* U_{\text{CW},00} + U_{\text{CCW},10}^* U_{\text{CW},10}) \\ &+ \frac{1}{2} e^{i\phi/2} \sin \theta (U_{\text{CCW},00}^* U_{\text{CW},01} + U_{\text{CCW},10}^* U_{\text{CW},11}) \\ &+ \sin^2 \frac{\theta}{2} (U_{\text{CCW},01}^* U_{\text{CW},01} + U_{\text{CCW},11}^* U_{\text{CW},11}). \end{aligned}$$

If we calculate the average value of $\langle i | \mathbf{U}_{\text{CCW}}^\dagger \mathbf{U}_{\text{CW}} | i \rangle$, letting $|i\rangle$ span all points on the Bloch sphere, the second term in the above equation becomes zero. We also have $\langle \cos^2 \theta/2 \rangle_{\text{ave}} = 1/2$. Then,

$$\begin{aligned} \langle i | \mathbf{U}_{\text{CCW}}^\dagger \mathbf{U}_{\text{CW}} | i \rangle_{\text{ave}} &= \frac{1}{2} (U_{\text{CCW},00}^* U_{\text{CW},00} + U_{\text{CCW},10}^* U_{\text{CW},10}) \\ &+ \frac{1}{2} (U_{\text{CCW},01}^* U_{\text{CW},01} + U_{\text{CCW},11}^* U_{\text{CW},11}) \\ &= \frac{1}{2} \text{Tr} \{ \mathbf{U}_{\text{CCW}}^\dagger \mathbf{U}_{\text{CW}} \} \end{aligned}$$

and

$$\begin{aligned} \left| \frac{1}{\sqrt{2}} (\psi_{\text{CW}} + \psi_{\text{CCW}}) \right|_{\text{ave}}^2 &= 1 + \frac{1}{2} \text{Re} \{ \text{Tr} \{ \mathbf{U}_{\text{CCW}}^\dagger \mathbf{U}_{\text{CW}} \} \} \cos \left(2\pi \frac{BS}{h/2e} \right). \end{aligned}$$

Under the time-reversal symmetry, $\mathbf{U}_{\text{CW}} = \mathbf{U}_{\text{CCW}}^{-1} = \mathbf{U}_{\text{CCW}}^\dagger$. Therefore, $\mathbf{U}_{\text{CCW}}^\dagger \mathbf{U}_{\text{CW}} = \mathbf{U}_{\text{CW}}^2$. In the case of spin rotation by the SOI, two elements in the diagonal positions of \mathbf{U}_{CW}^2 are complex conjugate to each other. Therefore,

$$\frac{1}{2} \text{Re} \{ \text{Tr} \{ \mathbf{U}_{\text{CW}}^2 \} \} = \frac{1}{2} \text{Tr} \{ \mathbf{U}_{\text{CW}}^2 \}.$$

APPENDIX C: EXPRESSION OF $\mathbf{R}_{\hat{\xi}}(\theta)$ FOR THE CUBIC DRESSELHAUS

Let us consider the spin rotation by the cubic Dresselhaus Hamiltonian $H_D^{(3)} = \beta_3 k^3 \{ \sigma_x \cos(3\varphi) + \sigma_y \sin(3\varphi) \}$. This can be understood as $\tilde{\mathbf{B}} = (\beta_3 k^3 \cos(3\varphi), \beta_3 k^3 \sin(3\varphi))$, with $\mathbf{k} = (k \cos \varphi, k \sin \varphi)$. We obtain $\hat{\xi} = (\cos(3\varphi), \sin(3\varphi))$ and $\theta = 2\beta_3 k^3 l / \hbar v_F = 4\beta_3 (m^*)^2 E_{\text{FL}} / \hbar^4$, where l is the length of the electron passage (segment) in the predetermined return orbitals (already scaled by the actual mean-free-path value ℓ).

The expression of the spin rotation operator for the cubic Dresselhaus Hamiltonian then becomes

$$\begin{aligned} \mathbf{R}_{\hat{\xi}}(\theta) &= \begin{pmatrix} \cos \left[\frac{2\beta_3 (m^*)^2 E_{\text{FL}}}{\hbar^4} \right] & -i e^{-3i\varphi} \sin \left[\frac{2\beta_3 (m^*)^2 E_{\text{FL}}}{\hbar^4} \right] \\ -i e^{3i\varphi} \sin \left[\frac{2\beta_3 (m^*)^2 E_{\text{FL}}}{\hbar^4} \right] & \cos \left[\frac{2\beta_3 (m^*)^2 E_{\text{FL}}}{\hbar^4} \right] \end{pmatrix}. \end{aligned}$$

APPENDIX D: CALCULATED RESULTS OF $\Delta\sigma$ UNDER THE RASHBA SOI FOR $L_\phi = 100$ AND 1000

In Fig. 6, we show image plots of the calculated $\Delta\sigma$ and the estimated statistical errors for it, $\delta\Delta\sigma$, as a function of the magnetic field B and spin rotation angle per the MFP value θ_R , with $L_\phi = 100$ and 1000 . We also show cuts of

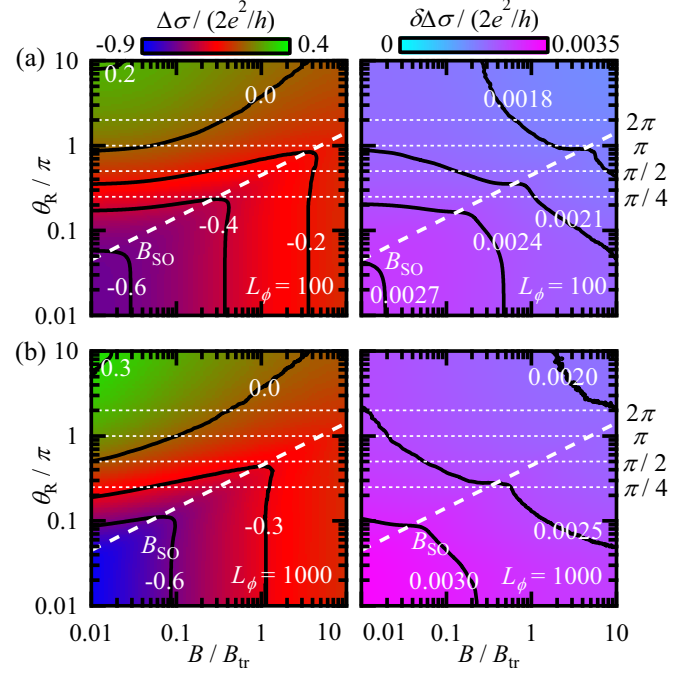


FIG. 6. (a), (b) Image plots of the calculated $\Delta\sigma$ (left) and the estimated statistical errors of $\Delta\sigma$, denoted as $\delta\Delta\sigma$ (right) as a function of the magnetic field B (abscissa) and spin rotation angle per the MFP value θ_R (ordinate). (a) $L_\phi = 100$; (b) $L_\phi = 1000$.

the image plots at $\theta_R = 0, \pi/4, \pi/2, \pi$, and 2π , as well as $B = 0$, to compare with the corresponding results by the Golub model [45] (Fig. 7).

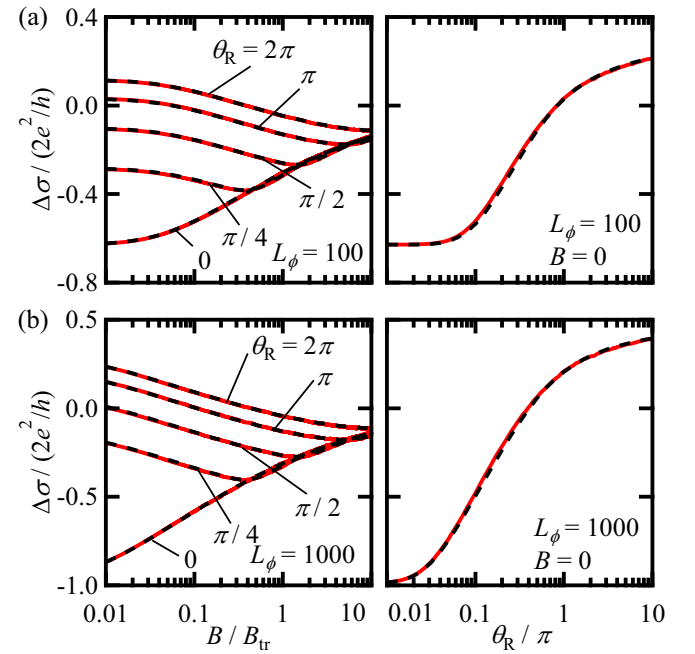


FIG. 7. (a), (b) (Left) Cuts (cross sections) of the image plot of $\Delta\sigma$ in Fig. 6 at $\theta_R = 0, \pi/4, \pi/2, \pi$, and 2π (red solid curves) together with the corresponding results by the Golub model [45] (black dashed curves). (a), (b) (Right) θ_R dependence of $\Delta\sigma$ calculated by our model (red solid curve) and the Golub model (black dashed curve) at $B = 0$. (a) $L_\phi = 100$; (b) $L_\phi = 1000$.

APPENDIX E: DERIVATION OF $\delta\Delta\sigma[i]$ VS $B[i]$

We can estimate the statistical deviation of $\Delta\sigma$, which is denoted as $\delta\Delta\sigma$, from the variance of $X_\nu(B)$ as

$$\begin{aligned}\delta\Delta\sigma(B) &= \frac{1}{\sqrt{N_{\text{orbit}}}} \sqrt{\langle [X_\nu(B)]^2 \rangle_{N_{\text{orbit}}} - \langle X_\nu(B) \rangle_{N_{\text{orbit}}}^2} \\ &< \frac{1}{\sqrt{N_{\text{orbit}}}} \sqrt{\langle [X_\nu(B)]^2 \rangle_{N_{\text{orbit}}}} \\ &= \frac{e^2 F_0}{2\pi^2 \hbar \sqrt{N_{\text{orbit}}}} \sqrt{\frac{\sum_{\nu=1}^{N_{\text{orbit}}} [x_\nu \cos(2\pi \frac{B S_\nu \ell^2}{h/2e})]^2}{N_{\text{orbit}}}} \\ &= \frac{e^2 F_0}{2\pi^2 \hbar \sqrt{N_{\text{orbit}}}} \sqrt{\frac{\sum_{\nu=1}^{N_{\text{orbit}}} x_\nu^2 [1 + \cos(4\pi \frac{B S_\nu \ell^2}{h/2e})]}{2N_{\text{orbit}}}} \\ &= \frac{e^2 F_0}{2\pi^2 \hbar \sqrt{N_{\text{orbit}}}} \sqrt{\frac{\sum_{\nu=1}^{N_{\text{orbit}}} x_\nu^2 + \sum_{\nu=1}^{N_{\text{orbit}}} x_\nu^2 \cos(2\pi \frac{B' S_\nu \ell^2}{h/2e})}{2N_{\text{orbit}}}},\end{aligned}$$

where $B' = 2B$. Letting $w_2[0, \dots, 2^N]$ be the histogram of x_ν^2 ($w_2[i] = \sum_{j=1}^{N_i} x_j^2$), where N_i is the number of loops belonging to the i th bin of the histogram, we find $\sum_{\nu=1}^{N_{\text{orbit}}} x_\nu^2 = w_2[0]_{\text{FFTed}}$ and $\sum_{\nu=1}^{N_{\text{orbit}}} x_\nu^2 \cos(2\pi \frac{B'[i] S_\nu}{h/2e}) = w_2[i]_{\text{FFTed}}$, with $B'[i] = \frac{i}{2^N} \times \frac{\pi B_{\text{tr}}}{\Delta S}$. Finally, we have

$$\delta\Delta\sigma[i] = \frac{e^2 F_0}{2\pi^2 \hbar \sqrt{N_{\text{orbit}}}} \sqrt{\frac{w_2[0]_{\text{FFTed}} + w_2[i]_{\text{FFTed}}}{2N_{\text{orbit}}}},$$

with

$$B[i] = \frac{B'[i]}{2} = \frac{i}{2^N} \times \frac{\pi B_{\text{tr}}}{2\Delta S}.$$

-
- [1] L. P. Gor'kov, A. I. Larkin, and D. E. Khmel'nitskii, *Pis'ma Zh. Eksp. Teor. Fiz.* **30**, 248 (1979) [*JETP Lett.* **30**, 228 (1980)].
- [2] D. E. Khmel'nitskii, *Physica B+C (Amsterdam)* **126**, 235 (1984).
- [3] G. Bergmann, *Phys. Rep.* **107**, 1 (1984).
- [4] S. Chakravarty and A. Schmid, *Phys. Rep.* **140**, 193 (1986).
- [5] T. Koga, J. Nitta, T. Akazaki, and H. Takayanagi, *Phys. Rev. Lett.* **89**, 046801 (2002).
- [6] J. B. Miller, D. M. Zumbühl, C. M. Marcus, Yu. B. Lyanda-Geller, D. Goldhaber-Gordon, K. Campman, and A. C. Gossard, *Phys. Rev. Lett.* **90**, 076807 (2003).
- [7] S. Faniel, T. Matsuura, S. Mineshige, Y. Sekine, and T. Koga, *Phys. Rev. B* **83**, 115309 (2011).
- [8] D. Spirito, L. Di Gaspere, F. Evangelisti, A. Di Gaspere, E. Giovine, and A. Notargiacomo, *Phys. Rev. B* **85**, 235314 (2012).
- [9] R. Moriya, K. Sawano, Y. Hoshi, S. Masubuchi, Y. Shiraki, A. Wild, C. Neumann, G. Abstreiter, D. Bougeard, T. Koga, and T. Machida, *Phys. Rev. Lett.* **113**, 086601 (2014).
- [10] G. M. Minkov, A. V. Germanenko, O. E. Rut, A. A. Sherstobitov, S. A. Dvoretzki, and N. N. Mikhailov, *Phys. Rev. B* **91**, 205302 (2015).
- [11] H. Nakamura, T. Koga, and T. Kimura, *Phys. Rev. Lett.* **108**, 206601 (2012).
- [12] F. V. Tikhonenko, A. A. Kozikov, A. K. Savchenko, and R. V. Gorbachev, *Phys. Rev. Lett.* **103**, 226801 (2009).
- [13] Z. Wang, D. K. Ki, H. Chen, H. Berger, A. H. MacDonald, and A. F. Morpurgo, *Nat. Commun.* **6**, 8339 (2015).
- [14] H. Yuan, M. S. Bahramy, K. Morimoto, S. Wu, K. Nomura, B.-J. Yang, H. Shimotani, R. Suzuki, M. Toh, Ch. Kloc, X. Xu, R. Arita, N. Nagaosa, and Y. Iwasa, *Nat. Phys.* **9**, 563 (2013).
- [15] R. Sei, T. Fukumura, and T. Hasegawa, *ACS Appl. Mater. Interfaces* **7**, 24998 (2015).
- [16] V. Deo, Y. Zhang, V. Soghomonian, and J. J. Heremans, *Sci. Rep.* **5**, 9487 (2015).
- [17] M. Kepenekian, R. Robles, C. Katan, D. Saporì, L. Pedesseau, and J. Even, *ACS Nano* **9**, 11557 (2015).
- [18] T. Kimura, T. Goto, H. Shintani, K. Ishizaka, T. Arima, and Y. Tokura, *Nature (London)* **426**, 55 (2003).
- [19] H. J. Xiang, Su-Huai Wei, M.-H. Whangbo, and Juarez L. F. Da Silva, *Phys. Rev. Lett.* **101**, 037209 (2008).
- [20] S. Hikami, A. I. Larkin, and Y. Nagaoka, *Prog. Theor. Phys.* **63**, 707 (1980).
- [21] S. V. Iordanskii, Yu. B. Lyanda-Geller, and G. E. Pikus, *Pis'ma Zh. Eksp. Teor. Fiz.* **60**, 199 (1994) [*JETP Lett.* **60**, 206 (1994)].
- [22] T. Nambu, S. Kawaji, K. Kuboki, Y. Kawaguchi, J. Yoshino, and H. Sakaki, *J. Phys. Soc. Jpn.* **53**, 682 (1984).
- [23] S. McPhail, C. E. Yasin, A. R. Hamilton, M. Y. Simmons, E. H. Linfield, M. Pepper, and D. A. Ritchie, *Phys. Rev. B* **70**, 245311 (2004).
- [24] A. Kawabata, *J. Phys. Soc. Jpn.* **49**, 628 (1980).
- [25] A. Kawabata, *J. Phys. Soc. Jpn.* **53**, 3540 (1984).
- [26] P. A. Lee and T. V. Ramakrishnan, *Phys. Rev. B* **26**, 4009 (1982).
- [27] V. M. Gasparyan and A. Yu. Zyuzin, *Fiz. Tverd. Tela (Leningrad)* **27**, 1662 (1985) [*Sov. Phys. Solid State* **27**, 999 (1985)].
- [28] M. I. Dyakonov, *Solid State Commun.* **92**, 711 (1994).

- [29] H.-P. Wittmann and A. Schmid, *J. Low Temp. Phys.* **69**, 131 (1987).
- [30] A. Zduniak, M. I. Dyakonov, and W. Knap, *Phys. Rev. B* **56**, 1996 (1997).
- [31] A. P. Dmitriev, V. Yu. Kachorovskii, and I. V. Gornyi, *Phys. Rev. B* **56**, 9910 (1997).
- [32] G. M. Minkov, A. V. Germanenko, V. A. Larionova, S. A. Negashev, and I. V. Gornyi, *Phys. Rev. B* **61**, 13164 (2000).
- [33] L. E. Golub, *Phys. Rev. B* **71**, 235310 (2005).
- [34] T. Koga, J. Nitta, and M. van Veenhuizen, *Phys. Rev. B* **70**, 161302 (2004).
- [35] S. Mineshige, S. Kawabata, S. Faniel, J. Waugh, Y. Sekine, and T. Koga, *Phys. Rev. B* **84**, 233305 (2011).
- [36] E. McCann, K. Kechedzhi, V. I. Fal'ko, H. Suzuura, T. Ando, and B. L. Altshuler, *Phys. Rev. Lett.* **97**, 146805 (2006).
- [37] B. A. Bernevig, J. Orenstein, and S.-C. Zhang, *Phys. Rev. Lett.* **97**, 236601 (2006).
- [38] See Supplemental Material at <http://link.aps.org/supplemental/10.1103/PhysRevE.95.023309> for information on all 147 885 return orbitals.
- [39] $L_\phi = v_F \tau_\phi / \ell$ in dimensionless quantity.
- [40] Note the different definition for the angle φ'_j here than in Eq. (21) of Ref. [32].
- [41] We use “cosft1()” function in Ref. [48]. Note that “cosft1(w)” replaces the array $w[0, \dots, 2^N]$ to $w[0, \dots, 2^N]_{\text{FFTed}}$, but all values are then shifted by a constant value $-w[0]/2$ assuming $w[2^N] = 0$ in the original array. Therefore, we have to add the constant value $w[0]/2$ to all the members of the converted array $w[0, \dots, 2^N]_{\text{FFTed}}$ before it is used in the present calculation.
- [42] We find $w_0[2^N] = 0$ if $N \geq 13$ in the present case using all 147 885 orbitals.
- [43] One can use any number of the closed loops (N_{orbit}) starting from $\nu = 1$ in [38] in the increasing order in ν as far as $N_{\text{orbit}} \leq 147, 885$.
- [44] This corresponds to $L_\phi = 10\ell$ in the actual experimental length.
- [45] The results of the Golub model here are obtained by reading $\exp(-x \frac{l_B}{l} - \frac{x^2}{2})$ as $\exp(-x \frac{l_B}{l} - \frac{x^2}{2})$ in $Q_N^{(m)}$, $S_N^{(m)}$, and $R_N^{(m)}$ of Ref. [33], where $\tilde{l} = l/(1 + \tau_{\text{tr}}/\tau_\phi)$.
- [46] This error arises from the approximation to use Bessel functions in Eqs. (26) and (27) of Ref. [33].
- [47] K. Yoshizumi, A. Sasaki, M. Kohda, and J. Nitta, *Appl. Phys. Lett.* **108**, 132402 (2016).
- [48] W. H. Press, S. A. Teukolsky, W. T. Vetterling, and B. P. Flannery, *Numerical Recipes in C++ : The Art of Scientific Computing* (Cambridge University Press, New York, 2002).
- [49] A. Sawada and T. Koga (unpublished).